Spectroscopy of Jet-Cooled Water Complexes with Coumarin 151: Observation of Vibronically Induced Conformational Barrier Crossing

Brian A. Pryor, Phillip M. Palmer, Peter M. Andrews, Mitchell B. Berger, and Michael R. Topp*

Department of Chemistry, University of Pennsylvania, Philadelphia, Pennsylvania 19104-6323

Received: January 27, 1998

Coumarin 151, when complexed 1:1 by a water molecule in a supersonic jet, develops two sets of resonances, based on features displaced by -45 cm^{-1} (species A) and -690 cm^{-1} (species B) from the uncomplexed molecule. The vertical ionization thresholds of these species differ by a much greater amount (0.5 eV) than the bound states, confirming that the attachment sites are functionally different. When two water molecules are present, there appears to be a single cluster type, having an origin shifted from the bare chromophore by -1214 cm^{-1}. In this case, fluorescence excitation spectra recorded simultaneously at two emission wavelengths show that the 2:1 species exhibit a Stokes shift for excitation energies ≥ 60 cm^{-1}. Also, above this energy barrier, the ionization energy shifts downward by >1000 cm^{-1}. The bare molecule also undergoes vibronically induced nonradiative relaxation, but this occurs at higher energies (i.e., >450 cm^{-1}) and results in a large *increase* in the effective ionization threshold. The fluorescence decay time of the 2:1 water aggregate, excited into the zero-point level of S_1, was found to be twice that of the bare molecule (6.7 ns vs 3.5 ns). Above the relaxation barrier, the decay time of the initial state rapidly decreased below the instrument resolution of 35 ps. On the other hand, the fluorescence decay time of the product state increased to $\approx$9.5 ns and remained constant up to >400 cm^{-1} excess vibrational energy.

1. Introduction

Much current work is directed toward understanding the interactions responsible for the solvent sensitivity of molecular fluorescence, in fluid solution, membranes, proteins, micelles, and other small particles, at interfaces, and in molecular clusters. Many models used to describe dynamical solvent shifts in solution involve the cumulative effect of a large number of molecules. However, molecular-scale models are needed to explain the effects of short-range intermolecular interactions in clusters, and in the refinement of models for extended solvents, where site-specific interactions such as hydrogen bonding play an important role.[1] This site-specific interaction sufficiently perturbs the electron distribution of molecules that, in many cases, it can lead to the reordering of electronic states and consequently large changes in photochemical behavior. From another point of view, a small molecule such as water can be used to probe charge density changes occurring when a large molecule to which it is attached becomes electronically excited, or ionized. It is particularly important to identify cases where the change in the electronic charge distribution causes the site equilibrium to shift, since the associated spectroscopic Stokes shift behavior can be used to probe activated barrier crossing and the shape of the binding potential energy surface. Direct measurements of the relaxation dynamics on a picosecond or faster time scale could provide a means to examine the factors constraining a molecule at a given hydrogen-bonding site.

Molecular clusters have for some time provided a means to study the emergence of "solvation" interactions, which can be addressed through the evolution of molecular properties with increasing cluster size. One focus of photochemical interest has been to identify the threshold number of molecules required for a reaction to take place. For example, it is known that up to five ammonia molecules are needed in a cluster with phenol, and three with 1-naphthol, to observe an excited-state proton-transfer reaction.[2−4] On the other hand, it is not known in sufficient detail to what degree these effects are caused by structural placement of the attached molecules, or by thermodynamic considerations. It is important to be able to specify the energy available to a given system through structured excitation spectra and, as far as possible, to relate reactivity to experimental measurements of the structure.[4−16]

Many cases involving strong intermolecular forces do not show significant relaxation effects at the 1:1 level. For example, the 1:1 complex of water with 3-aminophthalimide shows vibrationally unrelaxed emission on a nanosecond time scale at a vibrational energy of 210 cm^{-1}.[17] Similar behavior is revealed in the spectra of 1:1 water complexes of 4-aminophthalimide[17] and Coumarin 152A.[18] Such behavior is most likely associated with the attachment of the first water molecule at a site whichthat is particularly stable with respect to electronic excitation. On the other hand, subsequent water molecules are not necessarily locked at a particular site on the chromophore, and are more susceptible to vibronically induced perturbation. Coumarin 151 (C151; 7-amino-4-trifluoromethylcoumarin) is one such case, as is demonstrated here.

Many coumarin derivatives, particularly those involving 6- or 7-amino groups, exhibit large changes in dipole moment when electronically excited,[19] and display large fluorescence Stokes shifts in polar solvents. In the case of C151, according to one study,[20] the dipole moment increases from the ground-state value of 5.7 D to 11.0 D in S_1. Molecules of this class are widely used as laser dyes, and the solvent sensitivity and time dependence of their emission spectra have been extensively studied, both on an ultrafast time scale and via computer

S1089-5639(98)00900-1 CCC: $15.00
Published on Web 04/17/1998

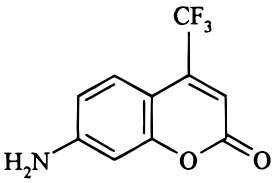

Coumarin 151
(7-amino-4-trifluoromethylcoumarin)

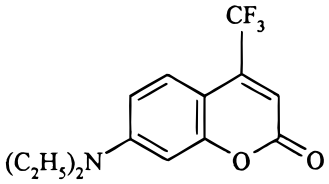

Coumarin 152A

simulations.[1,20−24] Despite their technical application as laser dyes, 7-amino coumarins are remarkably weakly fluorescent in some solvents.[20,25] Thus, C151, which fluoresces with high efficiency (i.e., $\Phi_F \geq 0.9$) in polar solvents, is much less efficient in nonpolar media ($\Phi_F = 0.19$ in hexane). This behavior has been attributed to coupling via a triplet state.[20] On the other hand, the dimethylamino and diethylamino derivatives, C152, and C152A, are strongly fluorescent in nonpolar solvents, but have much lower fluorescence quantum yields in alcohols and water. This behavior may be due to the stabilization of a TICT state.[20] In support of this, the more rigid cyclic derivative C153 is strongly fluorescent in most solvents. These divergent solvent effects provide additional motivation to study this interesting series of molecules in greater detail. The supersonic jet environment provides a valuable means to examine the electronic level structure of the isolated molecules, and its perturbation as they cluster with increasing numbers of "solvent" species in different configurations.

2. Experimental Section

(a) Fluorescence Experiments. Experiments reported here involved fluorescence excitation and electronic hole-burning spectroscopy. The latter experiments involved a strong tunable pump pulse and a weak fixed-wavelength pulse, separated by ≈500 ns (see Figure 1 (left)). Fluorescence signals were recorded in the same experiment from both pulses.[26,27] The hole-burning sequence involved wavelength scanning the first laser, from which our detector recorded together the saturated fluorescence excitation spectrum of all species present in the jet. The fixed probe pulse was tuned to the electronic origin resonance of the species being studied. Changes in this second signal, induced by scanning the first laser, reflected the saturated absorption spectrum of the species selected. The ratio of the two therefore represents the fluorescence quantum yield. The delay between pulses was ≈500 ns, which allowed sufficient time for the electronics to recover between pulses without the need for gating. These nanosecond-domain experiments used a 10 Hz Nd:YAG laser to pump an oscillator−amplifier dye laser, the output of which was passed through a self-tracking second harmonic generator. The hole-burning work also used a frequency-doubled dye laser pumped by the 532 nm output from an actively mode-locked Nd:YAG laser. This was continuously pumped, but acoustooptically Q-switched, in conjunction with the stronger Nd:YAG laser.

Our procedures for picosecond time-domain fluorescence spectroscopy, employing a time-correlated single-photon counter (TCSPC), have been described elsewhere.[28,29]

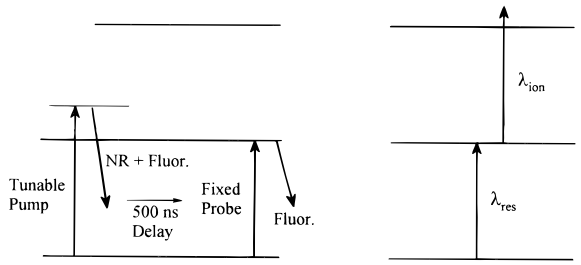

Fluorescence Hole Burning Two-Color Near-Threshold Photoionization

Figure 1. (left) Irradiation scheme for electronic hole-burning spectroscopy, using fluorescence detection. (right) Irradiation scheme for near-threshold two-photon ionization spectroscopy, using mass-resolved cation detection.

TABLE 1: Threshold Ionization Conditions for Coumarin 151 and Its $n = 1$, 2 Water Complexes[a]

species	S_1 energy (eV)	$\lambda(S_1 \rightarrow \text{ion})$	IE (eV)
Coumarin 151	3.55[b]	275	8.06
water $n = 1$ (A; −45 cm^{-1})	3.54	268	8.17
water $n = 1$ (B; −689 cm^{-1})	3.46	295	7.66
water $n = 2$ (origin; −1214 cm^{-1})	3.40	276	7.89
water $n = 2$ ($E_{vib} \geq 66$ cm^{-1})	[3.41]	284	⩽7.78[c]

[a] All measurements were made under dc field conditions of ≈200 V cm^{-1}. This implies that the values reported for the thresholds are low by ≤0.02 eV.[33] [b] 28 622 cm^{-1}. [c] The ionization energy of the product state from the ground-state surface is not known. The number given includes the energy of the barrier in the S_1 state, and therefore represents an upper limit.

(b) Mass-Resolved Spectroscopy. Coumarin 151 binds particularly strongly to water molecules, so that the experiment required drying the crystalline sample and the carrier gas. Considering this strong affinity, vapor pressure correlations, often used to estimate the aggregation levels for nonpolar clusters, are not reliable. Instead, mass-resolved spectroscopy is needed to identify the species present. The apparatus involved two dye lasers, both pumped by 532 nm pulses.[30] One source generated $S_0 \rightarrow S_1$ resonant pulses, λ_{res}, via a grazing-incidence grating, LDS 698 dye, and a self-tracking BBO frequency doubler. The second laser, in oscillator−amplifier configuration, generated near-threshold ionization pulses, λ_{ion}, in the range 270−305 nm (see Figure 1 (right)). Nd:YAG fourth-harmonic radiation (266 nm) was also used for the ionization step, in two-color mode. All the mass-resolved ionization data were calibrated in wavenumber and mass against an internal standard of anthracene.[31,32]

Ionization threshold data for the species studied are listed in Table 1. Although using ionizing photons well above the threshold caused some fragmentation, tuning this photon to a region <500 cm^{-1} above threshold in each case allowed us to isolate the parent ions for each cluster type. In each case, we are sure that the recorded masses correspond to the species actually excited. Referring to Table 1, our dc field ionization conditions reduce the measured ionization energies below the true values by ≤0.02 eV,[33] but still provide an excellent basis for comparison. Also, it should be noted that, for the isolated molecule, the ionization threshold was sharp (i.e., ≪0.02 eV), whereas for water complexes, the observed spectral widths in our experiment were ≤0.03 eV. This width is presumably due to Franck−Condon effects representing changes in equilibrium structure between the S_1 state and the ion. Although we have not found a reference value for C151, the measured value of 8.06 eV for the sharp threshold can be compared with the value

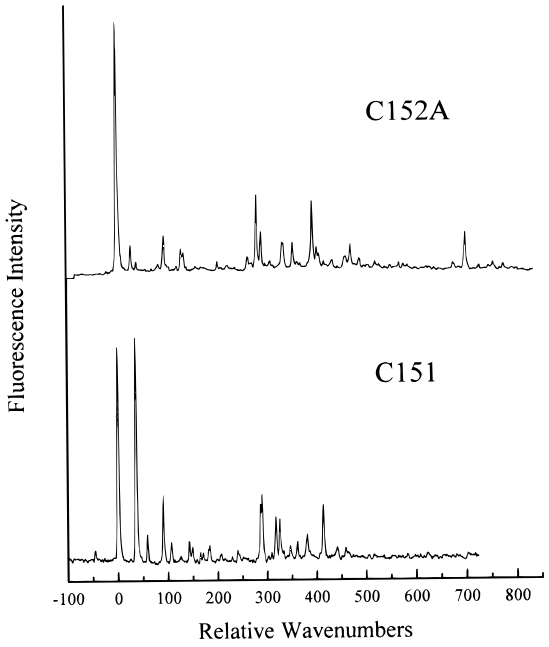

Figure 2. (lower) Fluorescence excitation spectrum of jet-cooled C151, recorded via unsaturated excitation and broad-band detection. (upper) Reference spectrum of C152A. The origins have been overlaid for comparison. Actual values are (C151) 28 622 cm^{-1} [36] and (C152A) 26 154 cm^{-1}.[36]

8.05 eV reported for the related species Coumarin 120 (7-amino-4-methylcoumarin).[34] Similarly, in other work,[18] we have measured the ionization energy of C152A (7.42 eV), which is close to that of its methyl analogue (Coumarin 1; 7-(diethylamino)-4-methylcoumarin; 7.38 eV).[34]

3. Results

(a) Isolated C151. The first reported study of coumarins under jet-cooled conditions was by Ernsting et al.[35] Consistent with its weak fluorescence in nonpolar media, the fluorescence excitation spectrum of jet-cooled C151 is found to be truncated above a vibrational energy of ≈450 cm^{-1},[35,36] unlike C152, C152A, or C153.[35,37] Figure 2 shows the fluorescence excitation spectrum of isolated C151 near the electronic origin of the $S_0 \rightarrow S_1$ transition (28 622 cm^{-1}, 349.4 nm). The excitation spectrum, obtained at low laser intensity where saturation is minimal, exhibits several medium to strong vibronic bands up to ≈450 cm^{-1}, some of which, including the strong resonance at 35 cm^{-1}, have been attributed to torsional vibration of the $-CF_3$ group.[36] This particular frequency assignment is consistent with the results of AM1 calculations we have performed, although we note that no similar band is seen in the excitation spectrum of C152A, which is shown for reference in Figure 2.[35,37] The two molecules have several key bands in common, near 100 cm^{-1} and at 250−425 cm^{-1}. The medium-strength feature near 680 cm^{-1}, which is characteristic of this type of coumarin molecule, is missing from the excitation spectrum of C151 because of the truncation above 450 cm^{-1}.

A hole-burning experiment served two purposes here. First, it confirmed that the feature at +35 cm^{-1} is due to a vibronic band of a single species. Second, it confirmed that the truncation of the excitation spectrum is due to a reduction in the fluorescence quantum yield. Thus, the spectra of Figure 3 were obtained as described in section 2 and Figure 1 (left), by setting the delayed probe laser pulse on resonance with the electronic origin transition of C151 and scanning the pump through the region shown. The two traces were recorded

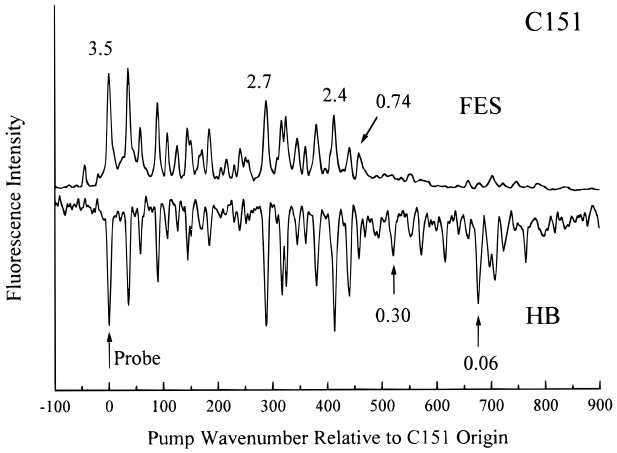

Figure 3. Fluorescence excitation spectrum (FES) of jet-cooled C151, combined with the hole-burning (HB) spectrum, both recorded in the same experiment and at higher laser intensity than for Figure 2. The numbers indicate the measured fluorescence decay times. The probe was resonant with the electronic origin, as indicated (↑).

TABLE 2: Fluorescence Decay Times of Jet-Cooled, Vibronically Excited Coumarin 151

excess energy, cm^{-1}	fluores decay time (ns)	excess energy, cm^{-1}	fluores decay time (ns)
0	3.5	409	2.4
35	4.8	439	0.80
89	4.3	455	0.75
180	2.9	520	0.30
289	2.7	676	0.06
318/324	3.0		

simultaneously by the same photomultiplier tube, using different boxcars to pick off signals coincident with the two laser pulses. The fluorescence excitation spectrum, recorded in this way (upper trace), is distorted by optical saturation effects, but allows a band-by-band comparison against the hole-burning trace. Despite the strong saturation, Figure 3 shows that all strong- and medium-intensity transitions appear in both spectra up to ≈450 cm^{-1}. This confirms that the resonances come from a single ground-state species. Above 450 cm^{-1}, the hole-burning spectrum, which measures absorption cross sections, shows continuation of the congested spectrum, including a strong band at 676 cm^{-1}, noted to be missing from Figure 2.

Results from time-resolved fluorescence measurements on isolated C151, some of which are labeled in Figure 3, are listed in Table 2. The emission time profile from the zero-point level of S_1 was exponential ($\tau_D \approx 3.5$ ns), and did not appear to depend on detection wavelength. The fluorescence decay times in the low-energy regime varied, much in the same way as anthracene or perylene, where there are varying degrees of singlet−triplet coupling.[28,38] For initial analysis, we employed a double-exponential fit, the numbers quoted in Table 2 and below being from the first (principal) component. At the highest energy for which we have obtained data for C151, corresponding to the strong absorption band at 676 cm^{-1}, we measured a relaxation time of ≈60 ps. This band was not observable above the noise in the excitation spectrum of Figure 2, but was identified via the picosecond transient feature in combination with the hole-burning spectrum of Figure 3. Nonradiative rate constants, estimated from the short-duration components of the fluorescence time profiles, were calculated according to the formula

$$k_{decay} = k_0 + k_d$$

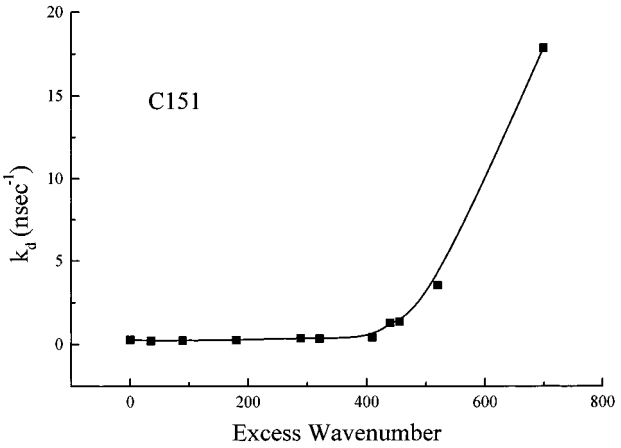

Figure 4. Plot of the nonradiative rate constant for jet-cooled C151 against excitation energy, measured by excess wavenumbers in S_1.

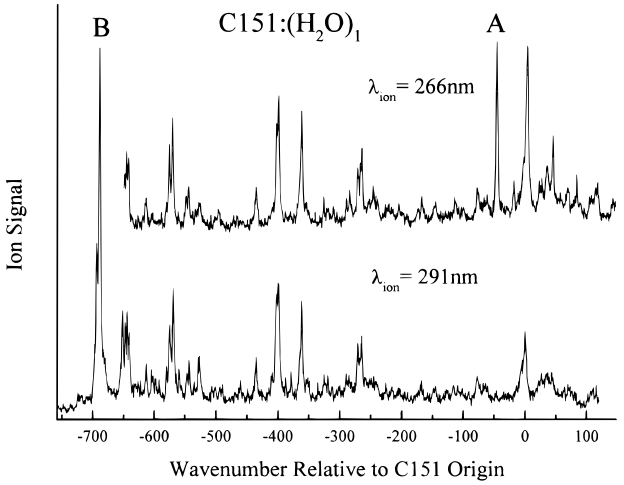

Figure 5. Mass-resolved excitation spectrum of C151/H_2O 1:1 as follows: (upper) λ_{ion} = 266 nm, so that both species "A" and "B" are seen; (lower) λ_{ion} = 291 nm, which is below the ionization threshold for species "A".

and plotted against excitation wavenumber in Figure 4. The quantity k_0 was taken to be the fluorescence decay rate constant following zero-point excitation. From the plot, we estimate an energy barrier of 400 cm^{-1}. These data reflect a familiar situation observed, for example, for *trans*-stilbene,[39−42] and 9,9′-bifluorenyl.[43,44] Both of those cases involve a barrier-crossing process leading to a nonfluorescent product, which also involves a major change in molecular structure. Unlike those cases, evidence from the literature suggests that the nonradiative relaxation of C151 involves singlet−triplet coupling.[20] Moreover, the elimination of fluorescence above 455 cm^{-1} suggests the presence of $\pi-\pi^*$ to n$-\pi^*$ singlet−triplet coupling. This is well-known to reduce excited singlet-state lifetimes in fluid solution to the picosecond domain in aromatic carbonyl derivatives such as benzophenone,[45,46] and in aza-aromatic molecules such as acridine.[47−50] However, few cases have been demonstrated under jet-cooled conditions, where singlet−triplet coupling reduces S_1 lifetimes to the picosecond domain. Moreover, it is rare to encounter a case where an intrinsically strongly fluorescent molecule—a laser dye in this case—has a dark relaxation channel at such a low energy above S_1.

Finally, in work not shown here, we have run the mass-resolved excitation spectrum of C151, setting the ionization laser just above the threshold energy, near 275 nm. The spectrum was a replica of that in the lower frame of Figure 2. That is, even in the mass-resolved two-color ionization excitation spectrum, the signal truncated above ≈450 cm^{-1}. Moreover, tuning the wavelength of the ionization laser to 266 nm did not change the outcome. From this, we deduce that there is a single ionization threshold for the molecule up to ≈450 cm^{-1}. Above that energy, a fast relaxation process crosses to an electronic surface from which a 266 nm, nanosecond-duration pulse is insufficient for ionization. This upshift in the ionization energy is contrasted below with the behavior of the 2:1 water aggregate.

(b) 1:1 Water Aggregate of C151. Molecular mechanics calculations predict four energy minima corresponding to hydrogen-bonded structures for a 1:1 water complex of C151. Three involve the amino group, and one structure involves the carbonyl group. These are analyzed later. Experimentally, when water is added, mass-resolved spectroscopy shows that multiple resonances develop to lower energy, the electronic origins of which are displaced −45, −689, and −1214 cm^{-1} from the bare molecule. The first two of these are due to 1:1 complexes, whereas the third is due to a 2:1 aggregate.

Figure 5 shows two excitation traces recorded via the $n = 1$ mass channel. For ionization wavelengths, λ_{ion}, in the range 295−272 nm, the lower spectrum was observed, which we label as species B. (The 272 nm limit was set by our dye laser.) Although further studies are needed to resolve the apparent inhomogeneous broadening, our experiments show that all the resonances for species B appear at about the same ionization threshold. We conclude that they are due to vibronic bands of one or more similar species, with proton tunneling being a distinct possibility for the splitting. On the other hand, if the ionization wavelength is reduced to 266 nm, several new bands appear, as shown in the upper trace. We place a preliminary estimate on the threshold ionization wavelength of 268 nm (37 300 cm^{-1}), giving an estimated ionization energy of 65 900 cm^{-1} (≡8.17 eV). This should be compared with the corresponding values for the B species of 295 nm (33 900 cm^{-1}) and 61 800 cm^{-1} (7.66 eV). Preliminary hole-burning experiments suggest that the sequence of bands headed by the feature at −45 cm^{-1} is due to a single progression of a species we have labeled "A". We have determined that the intense band near 0 cm^{-1} displacement is due to the 1:1 complex, and not to cross talk from the bare molecule channel.

The large difference in ionization energy between the A and B species, ≈0.5 eV, suggests a radical difference in the response of the attachment sites to electron promotion. The higher ionization energy of the A species is consistent with a hydrogen bond to the nitrogen atom, since the nonbonded electron density at that atom decreases substantially upon electron promotion.[22] We do not know the structure corresponding to species B. However, in view of the large stabilization energy in S_1 and the ion, and the predictions of molecular structure calculations, it is likely that the water molecule is attached to the carbonyl group (see later).

(c) 2:1 Water Aggregate of C151. The two fluorescence excitation spectra in Figure 6 were recorded simultaneously, using different photomultipliers connected to separate boxcar channels. One was mounted on a monochromator set at 380 ± 5 nm, and the other, behind a color filter, was detected $\lambda >$ 450 nm. This approach allowed an objective comparison of the two traces, minimizing possible contributions from systematic fluctuations. If the fluorescence spectrum had been independent of excitation energy, the two parts of Figure 6 would have the same shape. However, excitation of the 2:1 species at >60 cm^{-1} above the electronic origin band leads to a greater relative amount of fluorescence in the long-wavelength region.

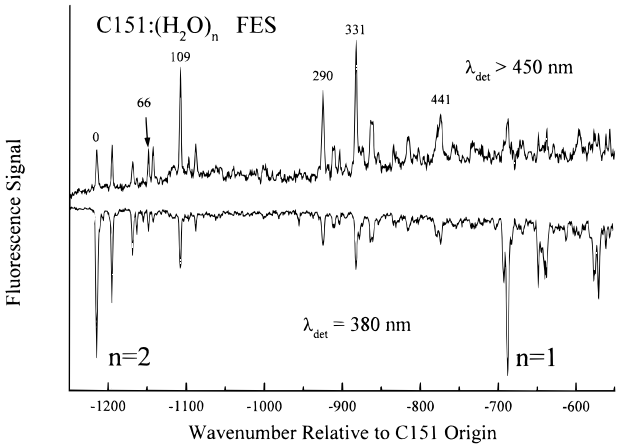

Figure 6. Fluorescence excitation spectrum in the region of the water 2:1 complex of C151, monitored at 380 ± 5 nm and >450 nm, and recorded simultaneously by two detectors.

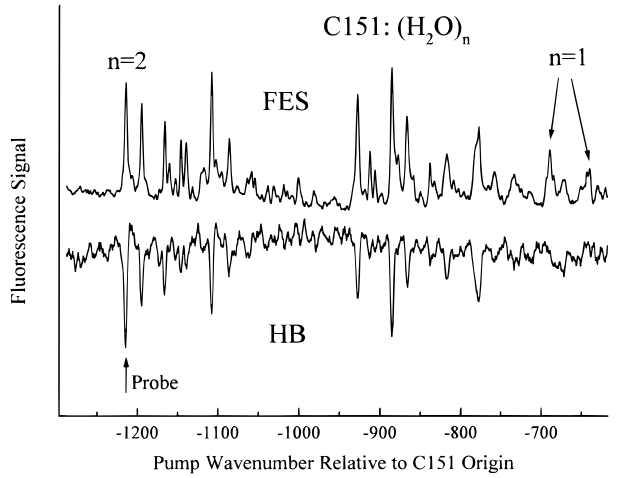

Figure 7. (HB) Fluorescence hole-burning spectrum obtained by probing the C151/$(H_2O)_2$ origin as shown by the arrow (↑). (FES) Fluorescence excitation intensity recorded from the saturated pump laser, 500 ns earlier than the probe.

As we show below, the features in the region below −700 cm^{-1} all correspond to the same level of aggregation, namely 2:1. One explanation of the observation in Figure 6 could be that two different 2:1 species are involved, which have different emission spectra. Electronic hole-burning resolved this issue, as shown in Figure 7. In that experiment, the delayed probe laser was tuned to the −1214 cm^{-1} feature (as indicated) while the saturating pulse was scanned through the region shown. Since all of the principal resonances appear in both spectra, we conclude that all bands in the region from −1214 cm^{-1} to just below −700 cm^{-1} originate from a common ground state.

The extent of the fluorescence Stokes shift is indicated in Figure 8, which shows emission spectra at 1 nm resolution, following excitation via the electronic origin and the strong 290 cm^{-1} band noted in Figure 6. At first, the shift does not appear large, certainly in comparison with the known condensed-phase behavior, but the amount of the shift is to some degree masked by the large widths of the spectra. Thus, electronic origin excitation leads to structured emission, having a Franck−Condon maximum near 385 nm, not including the 0−0 transition at 364.9 nm, and a half-intensity point near 410 nm. On the other hand, the emission following excitation at +290 cm^{-1} has a relatively sharp onset near 370 nm, a maximum at ≈400 nm, and a half-intensity point near 440 nm. The extent of the red shift, based on the centers of gravity of the two spectra, is

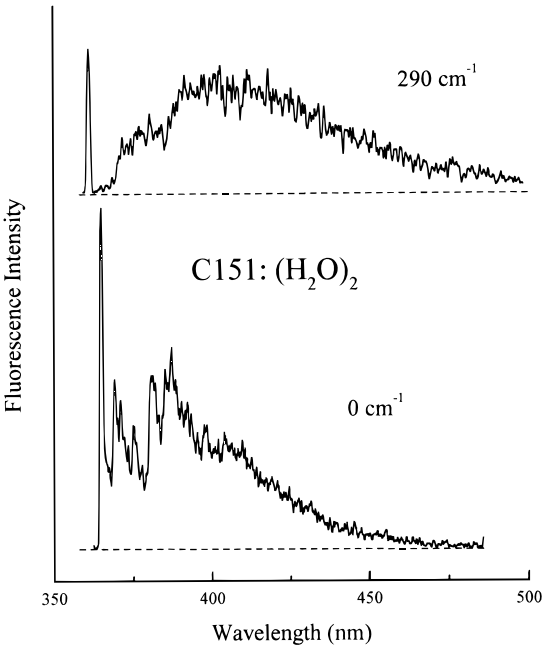

Figure 8. Dispersed fluorescence spectra for C151/$(H_2O)_2$ recorded for two different excitation conditions, below and above the energy barrier. Spectra were normalized to the same area, except for the scattered light peak in the upper trace.

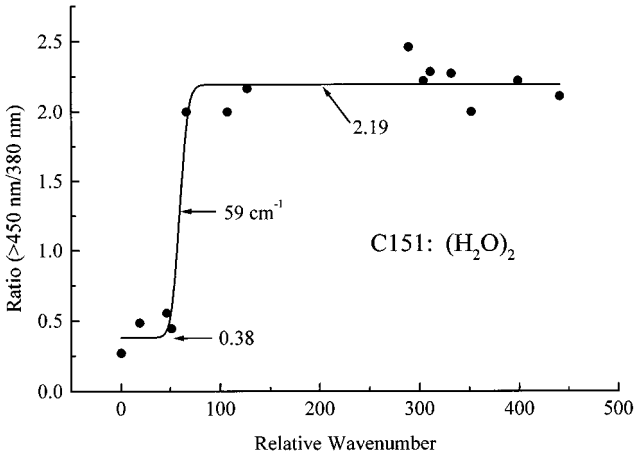

Figure 9. Ratios of the excitation band intensities from the two spectra shown in Figure 6. The fit to a sigmoidal curve suggests the presence of an energy barrier to relaxation near 59 cm^{-1}.

≥1500 cm^{-1}, which is much greater than for other nonreactive systems under jet conditions, except for possibly bianthryl/water.[51]

Figure 9 shows a plot of the band-by-band intensity ratio of the two excitation spectra in Figure 6, fit to a sigmoidal curve. In the region ≤60 cm^{-1}, the excitation resonances detected near 380 nm are more than twice as strong as those detected in the long-wavelength region, giving the ratio shown of ≈0.38. Above 60 cm^{-1}, the long-wavelength emission intensity exceeds that at 380 nm by a factor of ≈2.2. Over a region <20 cm^{-1} wide and centered at 59 cm^{-1}, therefore, the band intensity ratio (>450 nm/≈380 nm) changes by a factor of ≈6. We assume that the midpoint of the curve represents the effective energy barrier to the relaxation process.

We have also recorded the fluorescence time profiles of the C151/$(H_2O)_n$ complexes ($n = 1, 2$). The 1:1 species (A) showed a fluorescence decay time of ≈6 ns, which is appreciably longer than for the uncomplexed molecule. Also, for the 2:1 species up to 51 cm^{-1}, the highest internal energy for which the initial

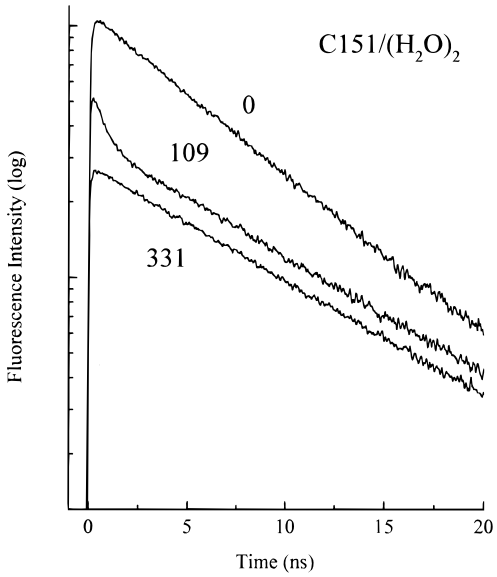

Figure 10. Fluorescence time profiles of C151/$(H_2O)_2$ measured at ≈380 nm for several different excitation positions: 0, 109, and 331 cm^{-1}, showing the evolution in decay time. The electronic origin decay is nearly pure exponential (6.9 ns (95%), 2.9 ns (5%)). The 109 cm^{-1} trace shows double-exponential (600 ps (50%), 9.6 ns (50%)) behavior due to the Stokes shift. The 331 cm^{-1} case showed a similar decay time (9.3 ns (100%)) due to product emission, but the Stokes shift occurred on a shorter time scale than our instrument response function.

TABLE 3: Fluorescence Decay Times of Vibronically Excited Coumarin 151/$(H_2O)_2$

excess energy (cm^{-1})	τ_f at 380 ± 5 nm (ns; ±2%)	excess energy (cm^{-1})	τ_f at 380 ± 5 nm (ns; ±2%)
0[a]	6.7	127	9.3
19	7.3	290	9.5
46	7.3	331	9.5
66	9.0, 1.2 (2:1)	352	9.5
72	9.1, 1.0 (7:1)	441	9.5
109	9.5, 0.6 (1:1)		

[a] −1214 from bare.

conformation appears stable, the fluorescence decay time was 6.7−7.3 ns. This is twice that for the bare molecule in the electronic origin region. In contrast, we note that C152 and C152A, which are electronically similar to C151, exhibit little vibrational dependence of the fluorescence decay time (≈6.1 ns) and little change in this quantity when complexed by water.[18]

In the intermediate energy region of 66−109 cm^{-1}, C151/$(H_2O)_2$ showed double-exponential fluorescence time profiles. Figure 10 shows three traces monitored at ≈380 nm following excitation at 0, 109, and 331 cm^{-1} above the S_1 origin. Other results are given in Table 3. The increase in fluorescence decay time from below the barrier (i.e., 6.7 ns at 0 cm^{-1}) to well above (i.e., 9.5 ns at 331 cm^{-1}), shows evidence for two different radiative lifetimes. This in turn suggests that the electronic structure associated with the initial and final sites is significantly different. Close to the barrier, the Stokes shift can be time-resolved by our apparatus, as seen in Figure 10 from the trace at 109 cm^{-1}. This shows a 600 ps component followed by a longer lifetime (9.5 ns) characteristic of the relaxed state. However, our experiment did not reveal double-exponential behavior above 109 cm^{-1}. Since the fluorescence decay time is constant in this region, evidently the rate of the Stokes shift was too fast for our experiment to follow. A pump−probe experiment with ≤1 ps resolution would be very useful to examine this process further.

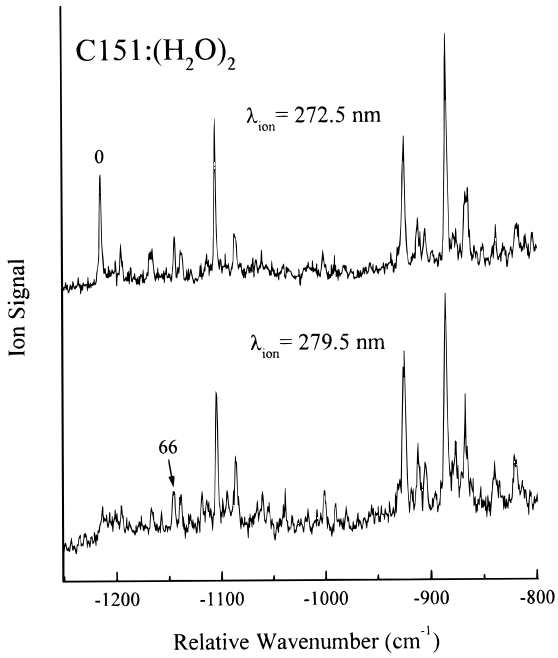

Figure 11. Mass-resolved excitation spectrum of C151/$(H_2O)_2$ as follows: (upper) λ_{ion} = 272.5 nm, which detects essentially the same spectrum as in the fluorescence excitation traces of Figure 6; (lower) scan of the same region, except with λ_{ion} = 279.5 nm, which is below the ionization threshold from the electronic origin transition.

To underline the above observation of electronic relaxation in the $n = 2$ species, we compare in Figure 11 the mass-resolved excitation spectrum of the 2:1 species, recorded for two ionization wavelengths, λ_{ion}. Although it was noted above that there is a single ground-state species at the 2:1 level, the experiments again reveal two ionization energies. The measured threshold, obtained in the usual way by tuning the first laser, λ_{res}, to the electronic origin at −1214 cm^{-1}, is near 273 nm. Thus, the upper frame in Figure 11 shows a spectrum, resembling the fluorescence excitation spectrum of Figure 6. The lower spectrum in Figure 11 could be observed by setting the wavelength of the ionization laser, λ_{ion}, at 275−284 nm. This spectrum is conspicuously missing the strong electronic origin transition, although the doublet feature at +66/72 cm^{-1} is evident. Moreover, the relative intensities of the remaining bands in the spectrum are about the same over this region of λ_{ion}. Evidently, the conformational relaxation process reduces the effective ionization threshold of this cluster by >1000 cm^{-1}.

4. Discussion

(a) Coumarin 151. Results presented here show that, for Coumarin 151 itself, the lifetime of the S_1 state decreases rapidly at energies >400 cm^{-1} above the origin. The diagram in Figure 12 qualitatively illustrates the relaxation sequence, in which interaction with a higher triplet state ($T_{n>1}$) depopulates S_1 above some threshold energy. Redistribution of the excess energy within T_1 on a picosecond or faster time scale also effectively removes the cross section for ionization, by shifting the Franck−Condon maximum to higher energies. Calculations of the energy level structure, using the AM1 semiempirical technique, confirm those previously reported[20,22] in that a low-lying triplet state (T_2) lies nearby in energy to the S_1 state, and thus may be the cause of the nonradiative decay. This picture is also consistent with the increased fluorescence quantum efficiency for C151 in polar solvents.[20,25] Thus, polar solvents may tend to stabilize the polar S_1 state, lowering it below the active triplet

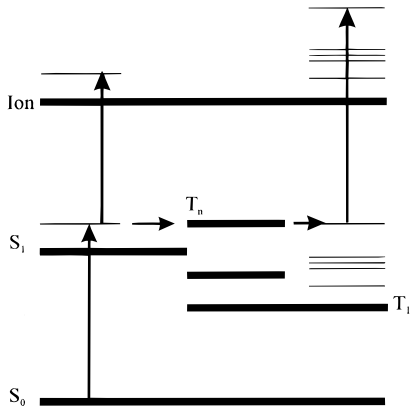

Figure 12. Energy level diagram schematically representing the increase ionization threshold of isolated C151, resulting from singlet−triplet coupling.

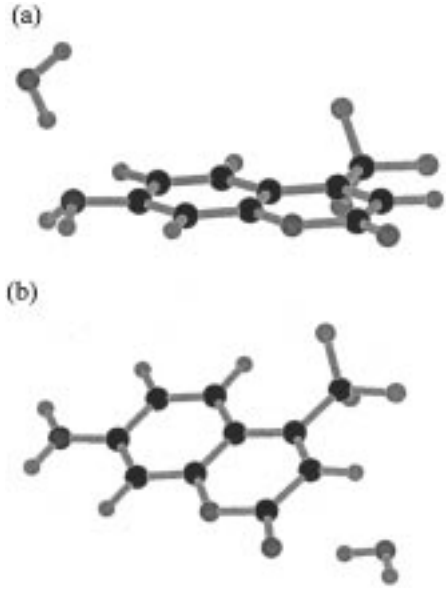

Figure 13. Two lowest energy structures for C151/H_2O calculated via molecular mechanics (MMFF).[53]

state and reducing the effects of intersystem crossing. A negative-ion photodetachment experiment would be quite useful to reveal the location of the low-lying nonfluorescent states of the bare molecule.[52]

(b) Structure Calculations for Coumarin 151/Water. We will shortly report the results of rotational coherence experiments on C152A which provide strong support for molecular mechanics and semiempirical predictions of the structures of different water complexes. However, C151 has not yielded rotational coherence data of sufficient quality to support such an analysis. Nonetheless, since the computational approach has proved useful for a similar molecule, the predictions, even at a semiquantitative level, are useful for illustration in this case.

Molecular mechanics calculations of different types predict several possible attachment sites for the first complexing water molecule on Coumarin 151, represented by potential energy minima of different depths. In the present case, we have minimized the structure of C151/H_2O via the Merck Molecular Force Field (MMFF; SPARTAN 5), and refined the two lowest energy results further, via a semiempirical procedure (PM3).[53] The MMFF structures, shown in Figure 13, involve (a) proton donation by a water molecule to the $-NH_2$ group at the 7-position and (b) to the carbonyl group. The PM3 calculation supported the MMFF structure of Figure 13 (b), although a PM3 calculation on the amino group site minimized the structure via proton donation from $-NH_2$ to the water molecule. This discrepancy between two approximate methods could readily be resolved via infrared double-resonance experiments probing the −N−H stretch region. Despite this difficulty, the sites represented by (a) and (b) in Figure 13 should undergo substantially different perturbations upon electronic promotion, considering the large increase in dipole moment (see below).

(c) Experimental Results for 1:1 Species. An important observation from the present work is the large difference in ionization energy depending on the location of the water molecule in the 1:1 species. One may note that the two conformers of indole/H_2O also have substantially different ionization energies ($\approx$2000 cm^{-1}).[54,55] An estimate of the change in the charge distribution of C151, induced by electronic excitation, can be made by considering changes in the partial charges on an atom-by-atom basis.[1,22] This approach has been used for correct predictions of molecular dipole moments.[22] Semiempirical calculations for C151 predict a substantial amount of excess electron charge on the nitrogen ($q = -0.38$) and carbonyl oxygen atoms ($q = -0.27$). Upon excitation, the charge rearrangement occurs with depletion of negative charge near the amine ($\Delta q(N) = +0.14$) and an increase in the vicinity of the CF_3 group. Our calculation, which used an AM1 routine from SPARTAN 5,[53] gives for the ground and excited dipole moments similar values to those calculated elsewhere ($\mu(S_0) =$ 5.7 D; $\mu(S_1) = 12.0$ D).[20,22]

Experimentally, we find two sets of absorption resonances for the 1:1 water adduct. One sequence (A), having an origin at -45 cm^{-1}, most likely represents attachment to the amino group, since the small shift suggests a more repulsive Coulombic interaction in the excited state. This species also exhibits an ionization energy of 8.17 eV, which is 0.11 eV higher than for C151 itself. This suggests that the binding energy is also considerably less in the ion. Indeed, AM1 calculations suggest a further reduction in the negative charge at the nitrogen atom, when the molecule is ionized (i.e., $\Delta q(S_0 \rightarrow \text{ion}) = +0.19$), and a dipole moment >10 D. However, the overall interaction is complex, and the change in this interaction upon excitation is difficult to model accurately. Also, one may note that the methanol 1:1 adducts of both perylene and anthracene show an increase of $\approx$0.1 eV in the ionization threshold, so that this observation is not unusual. The significant observation about C151/water is that the two sets of conformers have greatly different ionization energies. Thus, the second set of resonances near -690 cm^{-1} (B) most likely represents attachment of water to the carbonyl group, in view of the large reduction in the ionization threshold to 0.4 eV lower than C151 itself.

A second observation on the 1:1 species (see Figure 5) is that, in addition to the strongest band at -689 cm^{-1}, there is a second resonance, at -694 cm^{-1}. Also, many of the low-energy excitation resonances are compound. One possible conclusion is that there is more than one attachment site, having similar spectroscopic properties. Electronic spectral hole-burning experiments could determine how many ground-state species are responsible, while infrared−ultraviolet double-resonance experiments will be able to examine the types of hydrogen bonding present.[56,57] However, in the absence of further information about the attachment site or the type of coordination of the water molecule at that site, one should also consider the possibility of splitting due to torsional tunneling of the water molecule. It can be seen, for example, from Figure 13 that structure in (b) could present a torsional barrier to a singly hydrogen-bonded water molecule.

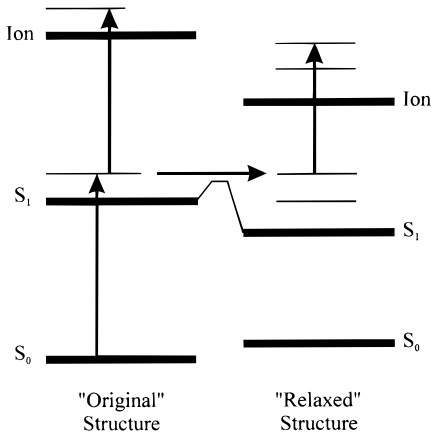

Figure 14. Energy level diagram schematically representing the decrease in ionization threshold of C151/$(H_2O)_2$ upon conformational barrier crossing.

(d) Experimental Results for 2:1 Species. Figure 14 represents, in terms of an energy level diagram, the picture we have obtained from the experiments on C151/$(H_2O)_2$. The ionization threshold of the "original" or ground-state structure is readily measured to be 7.89 eV. Following barrier crossing and relaxation, the "relaxed" structure is reached. Since relaxation occurs, we assume that the equilibrium energy of this species is lower than the original. At the excitation energy above the barrier, the population is redistributed into a dense manifold region of the S_1 state of the relaxed species—we know that this species has a lifetime of 9.5 ns. Ionization takes place to the corresponding Franck−Condon region of the ion, which occurs at a lower total energy than for the original structure—the onset was estimated at 7.78 eV. This picture again shows, like the 1:1 data, that the vertical ionization energy depends critically on the attachment site of the water molecule, relative to the coumarin. It is particularly noteworthy that an activation energy of only 60 cm^{-1} results in >1000 cm^{-1} reduction in ionization energy.

The observed relaxation process in C151/$(H_2O)_2$ happens at a lower activation energy than for nonradiative processes we have observed in other systems. For example, we have observed a Stokes shift in complexes of the aromatic hydrocarbon perylene ($C_{20}H_{12}$) with some *n*-alkyl halides.[58−61] In perylene/1-chlorobutane, we could detect three distinct structures at the 1:1 level, which were simultaneously present for a given set of conditions. Moreover, vibronic excitation (355 cm^{-1}) of two of the three conformers caused emission spectra to shift, suggesting the coupling of these sites via vibrational energy redistribution. The resulting small Stokes shifts of ≈80 cm^{-1} could be detected, because the spectra were not subject to large broadening. Also, the spectrum of one conformer chlorobutane/perylene showed a low-frequency mode progression suggesting a metastable structure constrained by a shallow well, similar to the present case of C151/$(H_2O)_2$. However, we concluded from that work that all three structures seen in the ground state were also present in the excited state, with little change in structure. In this case, the barrier to conformational change was not determined beyond an upper limit of 355 cm^{-1}.

Another Stokes shift case is the 1:1 complex of perylene with *p*-dichlorobenzene.[62] Here, only one ground-state structure appears to be present under jet-cooled conditions, the structure of which was shown by rotational coherence data to involve an overlapped parallel-plane conformation in which the molecular long axes are perpendicular. The Stokes shift here is much greater than for the alkyl halide case, at ≈400 cm^{-1}, although the activation barrier is still ≤350 cm^{-1}. Both this and the alkyl halide case involve strongly bound dimeric complexes not subject to large-amplitude motion, resulting in simple excitation spectra, and highly resolved rotational coherence data.

The observed activation energy of 60 cm^{-1} in the present case is the most direct evidence we have obtained for such a process. However, unlike the above two examples, the relevant structural conformations have yet to be determined. Recently, we have reported successful studies, combining rotational coherence spectroscopy with structure calculations for simple complexes of polycyclic aromatic molecules with polar adduct species.[17,62−64] We have attempted to use rotational coherence spectroscopy to analyze the structure of C151/$(H_2O)_2$. Indeed, the data, which are not shown here, suggest values of the rotational constants, as follows: $A + B = 790 \pm 50$ MHz; $C = 220 \pm 20$ MHz, based on a purely mathematical fit. However, we do not consider these data to be of sufficient precision for a direct structure assignment, especially since they could equally well fit both 1:1 and 2:1 structures. Moreover, C151 itself did not yield useful rotational coherence data, in part because of the high rotational asymmetry. Therefore, a structural model for this molecule would need to come from computations, the accuracy of which is weakened by the large change in dipole moment from $S_0 \rightarrow S_1$.

If one assumes that the two water molecules are present as a hydrogen-bonded dimer, it is possible to assert that in the $n = 2$ species, these cannot be involved in a hydrogen bond to the amino group. Simulations show that, since the NH_2 group is on the *A* axis of the bare molecule, such an attachment would cause the species to be a near-prolate top having a parallel transition. This would give rise to strong *J*-type transients, completely at variance with the experimental data. On the other hand, attachment of the water dimer in the vicinity of the α-pyrone ring near the oxygen atoms could give rise to rotational constants consistent with experiment. A further potential complication is that we know that the excited state of the $n = 2$ species is constrained only by a 60 cm^{-1} barrier, suggesting a weak restraining potential. It is therefore likely that a rigid-rotor model is not completely suitable for this species.

We will show in a forthcoming paper that rotational coherence spectroscopy can be used, in conjunction with molecular mechanics calculations, to analyze the structures of several derivatives of Coumarin 151, and some of their hydrogen-bonded complexes. Coumarin 151 itself, however, appears not to be well suited for such a study. Clearly, more detailed spectroscopic analysis is needed both to assign the base structure of the aggregate and to suggest a relaxation pathway.

5. Conclusion

In this work, we have demonstrated that different conformations of the $n = 1$ complex of C151 exhibit substantially different ionization energies. Moreover, the single conformation of the $n = 2$ complex exhibits vibronically induced relaxation leading to a fluorescence Stokes shift and a reduction in the ionization energy. These preliminary measurements set the stage for a more detailed examination of the relaxation process, including stimulated emission pumping experiments to follow vibrational relaxation dynamics, and pump−probe threshold ionization experiments to study the barrier-crossing process. There is an important need for better structural data, particularly about the changes in hydrogen-bond strength which may be induced by electronic excitation. These can be obtained via infrared−optical double-resonance techniques.

In a forthcoming paper, we will further explore the structure predictions of molecular mechanics and semiempirical quantum

mechanical techniques for derivatives of C151, for both the isolated molecules and some water complexes. An important distinction between those cases and C151 itself is that good quality rotational coherence data have already been obtained, for both uncomplexed molecules and some of their water complexes. This will aid greatly in assignment of the structures. Considering the early stage of refinement of conformational calculations, especially with respect to molecules having multiple functional groups, it remains a high priority to establish experimentally verifiable structural models.

Acknowledgment. This work was supported by the National Science Foundation (CHE-95-21362).

References and Notes

(1) Kumar, P. V.; Maroncelli, M. *J. Chem. Phys.* **1995**, *103*, 3038.
(2) Breen, J. J.; Peng, L. W.; Willberg, D. M.; Heikal, A.; Cong, P.; Zewail, A. H. *J. Chem. Phys.* **1990**, *92*, 805.
(3) Steadman, J.; Syage, J. A. *J. Chem. Phys.* **1990**, *92*, 4630.
(4) Siebrand, W.; Zgierski, M. Z.; Smedarchina, Z. K.; Vener, M.; Kaneti, J. *Chem. Phys. Lett.* **1997**, *266*, 47.
(5) Cheshnovsky, O.; Leutwyler, S. *J. Chem. Phys.* **1988**, *88*, 4127.
(6) Droz, T.; Knochenmuss, R.; Leutwyler, S. *J. Chem. Phys.* **1990**, *93*, 4520.
(7) Kim, S. K.; Bernstein, E. R. *J. Phys. Chem.* **1990**, *94*, 3531.
(8) Kim, S. K.; Li, S.; Bernstein, E. R. *J. Chem. Phys.* **1991**, *95*, 3119.
(9) Moog, R. S.; Maroncelli, M. *J. Phys. Chem.* **1991**, *95*, 10359.
(10) Moog, R. S.; Burozski, N. A.; Desai, M. M.; Good, W. R.; Silvers, C. D.; Simon, J. D. *J. Phys. Chem.* **1991**, *95*, 8466.
(11) Hineman, M. F.; Brucker, G. A.; Kelley, D. F.; Bernstein, E. R. *J. Chem. Phys.* **1992**, *97*, 3341.
(12) Plusquellic, D. F.; Tan, X.-Q.; Pratt, D. W. *J. Chem. Phys.* **1992**, *96*, 8026.
(13) Fee, R. S.; Maroncelli, M. *Chem. Phys.* **1994**, *183*, 235.
(14) Syage, J. A. *J. Phys. Chem.* **1995**, *99*, 5772.
(15) Kim, S. K.; Breen, J. J.; Willberg, D. M.; Peng, L. W.; Heikal, A.; Syage, J. A.; Zewail, A. H. *J. Phys. Chem.* **1995**, *99*, 7421.
(16) Humphrey, S. J.; Pratt, D. W. *J. Chem. Phys.* **1996**, *104*, 8332.
(17) Pryor, B. A.; Palmer, P. M.; Andrews, P. M.; Berger, M. B.; Troxler, T.; Topp, M. R. *Chem. Phys. Lett.* **1997**, *271*, 19.
(18) Pryor, B. A.; Andrews, P. M.; Palmer, M. B.; Topp, M. R. Manuscript in preparation.
(19) Rettig, W.; Klock, A. *Can. J. Chem.* **1985**, *63*, 1649.
(20) Rechthaler, K.; Köhler, G. *Chem. Phys.* **1994**, *189*, 99.
(21) Maroncelli, M.; Fleming, G. R. *J. Chem. Phys.* **1987**, *86*, 6221.
(22) McCarthy, P. K.; Blanchard, G. J. *J. Phys. Chem.* **1993**, *97*, 12205.
(23) Stratt, R. M.; Maroncelli, M. *J. Phys. Chem.* **1996**, *100*, 12981.
(24) Horng, M.-L.; Gardecki, J. A.; Maroncelli, M. *J. Phys. Chem. A* **1997**, *101*, 1030.
(25) Jones, G.; Jackson, W. R.; Choi, C.; Bergmark, W. R. *J. Phys. Chem.* **1985**, *89*, 294.
(26) Wittmeyer, S. A.; Topp, M. R. *Chem. Phys. Lett.* **1989**, *163*, 261.
(27) Wittmeyer, S. A.; Topp, M. R. *Chem. Phys. Lett.* **1990**, *171*, 29.
(28) Kaziska, A. J.; Wittmeyer, S. A.; Topp, M. R. *J. Phys. Chem.* **1991**, *95*, 3663.
(29) Troxler, T.; Smith, P. G.; Stratton, J. R.; Topp, M. R. *J. Chem. Phys.* **1994**, *100*, 797.
(30) Palmer, P. M.; Topp, M. R. *Chem. Phys. Lett.*, in press.
(31) Lambert, W. R.; Felker, P. M.; Syage, J. A.; Zewail, A. H. *J. Chem. Phys.* **1984**, *81*, 2195.
(32) Palmer, P. M.; Topp, M. R. Manuscript in preparation.
(33) Lipert, R. J.; Colson, S. D. *J. Chem. Phys.* **1990**, *92*, 3240.
(34) Redchenko, V. V.; Safronov, A. I.; Kirpichenok, M. A.; Grandberg, I. I.; Traven′, V. F. *J. Gen. Chem. USSR* **1992**, *62*, 2313.
(35) Ernsting, N. P.; Asimov, M.; Schaefer, F. P. *Chem. Phys. Lett.* **1982**, *91*, 231.
(36) Choo, J.; Kim, T.-S.; Choi, Y. S. *Bull. Korean Chem. Soc.* **1996**, *17*, 461.
(37) Taylor, A. G.; Bouwman, W. G.; Jones, A. C.; Guo, C.; Phillips, D. *Chem. Phys. Lett.* **1988**, *145*, 71.
(38) Felker, P. M.; Zewail, A. H. *J. Chem. Phys.* **1985**, *82*, 2975.
(39) Rothenberger, G.; Negus, D. K.; Hochstrasser, R. M. *J. Chem. Phys.* **1983**, *79*, 5360.
(40) Doany, F. E.; Heilweil, E. J.; Moore, R.; Hochstrasser, R. M. *J. Chem. Phys.* **1984**, *80*, 201.
(41) Felker, P. M.; Zewail, A. H. *J. Phys. Chem.* **1985**, *89*, 5402.
(42) Baskin, J. S.; Bañares, L.; Pedersen, S.; Zewail, A. H. *J. Phys. Chem.* **1996**, *100*, 11920.
(43) Lee, M.; Hochstrasser, R. M. *Chem. Phys. Lett.* **1988**, *153*, 1.
(44) Smith, P. G.; Gnanakaran, S.; Kaziska, A. J.; Motyka, A. L.; Hong, S. M.; Hochstrasser, R. M.; Topp, M. R. *J. Chem. Phys.* **1994**, *100*, 3384.
(45) Hochstrasser, R. M.; Lutz, H.; Scott, G. W. *Chem. Phys. Lett.* **1974**, *24*, 162.
(46) Anderson, R. W.; Hochstrasser, R. M.; Lutz, H.; Scott, G. W. *Chem. Phys. Lett.* **1975**, *32*, 204.
(47) Mataga, N.; Tsuno, S. *Bull. Chem. Soc. Jpn.* **1957**, *30*, 368.
(48) Bowen, E. J.; Holder, N. J.; Woodger, G. B. *J. Phys. Chem.* **1962**, *66*, 2491.
(49) Lin, H.-B.; Topp, M. R. *Chem. Phys.* **1979**, *36*, 365.
(50) Diverdi, L. A.; Topp, M. R. *J. Phys. Chem.* **1984**, *88*, 3447.
(51) Fujiwara, T.; Fujimura, Y.; Kajimoto, O. *Chem. Phys. Lett.* **1996**, *261*, 201.
(52) Schiedt, J.; Weinkauf, R. *Chem. Phys. Lett.* **1997**, *266*, 201.
(53) SPARTAN version 5.0, Wavefunction Inc., 18410 Von Karman Ave., #370, Irvine, CA 92715 USA.
(54) Hager, J.; Ivanco, M.; Smith, M. A.; Wallace, S. C. *Chem. Phys.* **1986**, *105*, 397.
(55) Tubergen, M. J.; Levy, D. H. *J. Phys. Chem.* **1991**, *95*, 2175.
(56) Tanabe, S.; Ebata, T.; Fujii, M.; Mikami, N. *Chem. Phys. Lett.* **1993**, *215*, 347.
(57) Pribble, R. N.; Zwier, T. S. *Faraday Discuss. Chem. Soc.* **1994**, *97*, 229.
(58) Motyka, A. L.; Wittmeyer, S. A.; Babbitt, R. J.; Topp, M. R. *J. Phys. Chem.* **1989**, *93*, 6322.
(59) Kaziska, A. J.; Shchuka, M. I.; Wittmeyer, S. A.; Topp, M. R. *J. Phys. Chem.* **1991**, *95*, 5017.
(60) Smith, P. G.; Topp, M. R. *Chem. Phys. Lett.* **1994**, *229*, 21.
(61) Troxler, T.; Stratton, J. R.; Smith, P. G.; Topp, M. R. *J. Chem. Phys.* **1994**, *101*, 9219.
(62) Pryor, B. A.; Andrews, P. M.; Palmer, P. M.; Topp, M. R. *Chem. Phys. Lett.* **1997**, *267*, 531.
(63) Andrews, P. M.; Pryor, B. A.; Palmer, P. M.; Topp, M. R. *Chem. Phys. Lett.* **1997**, *265*, 224.
(64) Andrews, P. M.; Pryor, B. A.; Berger, M. B.; Palmer, P. M.; Topp, M. R. *J. Phys. Chem. A* **1997**, *101*, 6222.